ORIGINAL RESEARCH

Biodynamer Nano-Complexes and -Emulsions for Peptide and Protein Drug Delivery

Yun Liu [ID][1,2], Timo Hamm[3], Thomas Ralf Eichinger[3], Walter Kamm[3], Heike Andrea Wieland[3], Brigitta Loretz [ID][1], Anna KH Hirsch[2,4], Sangeun Lee [ID][1,2], Claus-Michael Lehr[1,2]

[1]Department of Drug Delivery Across Biological Barriers, Helmholtz Institute for Pharmaceutical Research Saarland (HIPS), Helmholtz Centre for Infection Research (HZI), Saarbrücken, Germany; [2]Department of Pharmacy, Saarland University, Saarbrücken, Germany; [3]Department of Research and Development, Sanofi-Aventis Deutschland GmbH, Frankfurt Am Main, Germany; [4]Department of Drug Design and Optimisation, Helmholtz Institute for Pharmaceutical Research Saarland (HIPS), Helmholtz Centre for Infection Research (HZI), Saarbrücken, Germany

Correspondence: Claus-Michael Lehr, Department of Drug Delivery Across Biological Barriers, Helmholtz Institute for Pharmaceutical Research Saarland (HIPS), Helmholtz Centre for Infection Research (HZI), Saarbrücken, Germany, Tel +49 681 98806-1000, Fax +49 681 98806 1009, Email Claus-Michael.Lehr@helmholtz-hips.de; Sangeun Lee, Department of Pharmacy, Saarland University, Saarbrücken, Germany, Tel +49 681 302 4764, Fax +49 681 302 2028, Email Sangeun.Lee@uni-saarland.de

Background: Therapeutic proteins and peptides offer great advantages compared to traditional synthetic molecular drugs. However, stable protein loading and precise control of protein release pose significant challenges due to the extensive range of physicochemical properties inherent to proteins. The development of a comprehensive protein delivery strategy becomes imperative accounting for the diverse nature of therapeutic proteins.

Methods: Biodynamers are amphiphilic proteoid dynamic polymers consisting of amino acid derivatives connected through pH-responsive dynamic covalent chemistry. Taking advantage of the amphiphilic nature of the biodynamers, PNCs and DEs were possible to be prepared and investigated to compare the delivery efficiency in drug loading, stability, and cell uptake.

Results: As a result, the optimized PNCs showed 3-fold encapsulation (<90%) and 5-fold loading capacity (30%) compared to DE-NPs. PNCs enhanced the delivery efficiency into the cells but aggregated easily on the cell membrane due to the limited stability. Although DE-NPs were limited in loading capacity compared to PNCs, they exhibit superior adaptability in stability and capacity for delivering a wider range of proteins compared to PNCs.

Conclusion: Our study highlights the potential of formulating both PNCs and DE-NPs using the same biodynamers, providing a comparative view on protein delivery efficacy using formulation methods.

Keywords: amphiphilic polymer, nanocomplex, double emulsion, pH-responsive, protein delivery, dynamic covalent chemistry

Introduction

Therapeutic proteins and peptides are attracting tremendous attention as future medicines because of their high specificity and potency, lower adverse effects compared to traditional synthetic drugs, and regulation of the biological processes more directly and specifically than nucleotide-based drugs.[1] However, therapeutic proteins and peptides suffer from many challenges limiting their bioavailability, such as potential short half-life, structural stability, poor membrane permeability, and immunogenicity, caused by high Mw and hydrophilicity with charges.[2] Given the potential impact of protein therapeutics, developing protein delivery systems to overcome such challenges offers great opportunities. Effective protein delivery systems need to demonstrate stability, efficient cargo loading, facilitate intracellular transport, and release the cargo at the target site in a controlled manner.[3]

As protein carriers, lipid, polymeric, and inorganic micro/nanoparticles have been developed.[4–6] As a type of protein-loaded particles,[7] polymeric NPs are designed to form with cargos via non-covalent interactions like hydrogen bonds, electrostatic,[8] hydrophobic,[9,10] or π-π stacking interactions.[11] For example, by simply mixing negatively charged proteins and water-soluble positively charged polymers, PNCs can be formed via electrostatic interactions. This method is simple in the formulation and maintains the biological activity of drugs in a reliable way;[12] however, only charged proteins and

Graphical Abstract
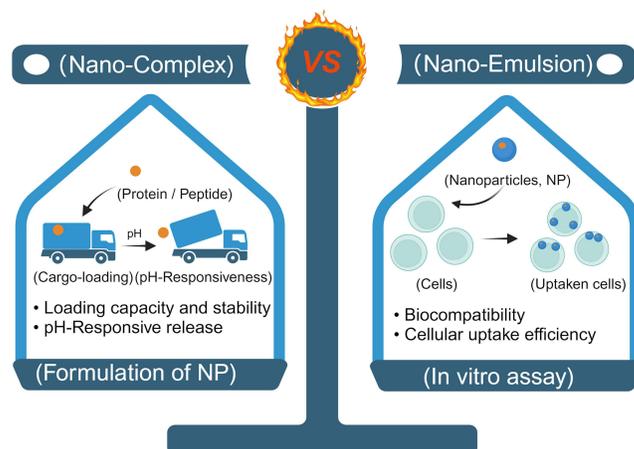
peptides can form PNCs with the oppositely charged polymers. As such, PNC formation is only possible for a specific protein and its corresponding polymer, requiring polymer design and high-level optimization processes depending on each protein cargo.

Emulsion-solvent evaporation method is also a widely used technique for polymeric NPs for protein delivery.[13,14] With the method, small-sized emulsion droplets can be formed based on the shear force at high pressures and cavitation effects by high energy approaches and high-pressure systems and devices.[15] In particular, DE-NPs, having hydrophilic compartments surrounded by hydrophobic compartments in the NPs, are possible to load hydrophilic and lipophilic drugs in the same delivery system.[16] In DE-NP formation, hydrophobic polymers are often used, but amphiphilic polymers, which have both hydrophobic and hydrophilic segments promoting surface activity and stability of multiple emulsions, are also applicable.[17] However, one critical limitation of the DE-NPs is that the LC% is generally low.[18] Likewise, each NP formulation method is known to have its own strengths and weaknesses. However, the methods can hardly be compared head-to-head because each method requires different polymer properties for a successful NP formulation.

Biodynamers are dynamic polymers polymerized by dynamic covalent chemistry between biomolecules.[19] As an example, we previously studied proteoid biodynamers, which are composed of amino acid hydrazides and HG-CA connected by pH-responsive dynamic covalent chemistry (acylhydrazones and imines). These acylhydrazones and imines between the monomers lead to the pH-responsive degradation of biodynamers under acidic microenvironments,[20] which is beneficial in cancer, inflammation, or infection targeting.[21–23] The proteoid biodynamers fold into a single-chain nanorod structure having a hydrophobic carbazole core and hydrophilic hexaethylene glycol shell, which endows the biodynamers with amphiphilicity.[24] Furthermore, modulating the compositions of 20 different amino acid hydrazide monomers makes it possible to control the physicochemical properties of biodynamers, such as charge, solubility, and hydrophilic–lipophilic balance.[25] Therefore, proteoid biodynamers are suitable not only for PNC formation because their physicochemical properties can be easily adjusted to suit the target cargo but also for DE-NP formation because of their amphipathicity. Resultingly, they are appropriate polymers to compare the two formulation methods, PNCs and DE-NPs.

Protein-loaded polymeric NPs offer notable advantages, including protection against protein degradation, enhanced stability, controlled release, and reduced dosing frequency.[26] However, challenges persist with polymeric NPs, such as potential toxicity associated with the solvent and stabilizer,[27] the elevated cost of particle production, the identification of suitable polymers to augment protein activity, and suboptimal drug EE%.[28] Polymeric PNCs and polymeric emulsions, as two distinct types of polymeric nanoparticles, each present a set of advantages and disadvantages. Charged PNCs exhibit notable attributes, including high encapsulation efficiency while preserving protein bioactivity,[29] however, a noteworthy challenge is encountered in terms of their inherent poor stability.[30] Nanoemulsion exhibits promise in encapsulating

poorly water-soluble drugs; however, the manufacturing process poses potential challenges, as it may influence the composition of the formulation and compromise drug stability.[31] The judicious selection of an appropriate technique is crucial, especially for protein delivery,[32] as it determines the pertinent applications and inherent advantages of the resulting nanoparticles.[33] A systematic comparison of protein delivery systems is imperative, encompassing considerations of loading efficiency, stability, and transport efficiency.

This study demonstrates the potential of amphiphilic biodynamers as promising nanoparticles for protein delivery while comparing two different formulation methods. Utilizing the easy controllability of biodynamers in charge and amphiphilicity, PNCs were first used to load oppositely charged protein cargos, OVA,[34] IH,[35] and GLP-1 via electrostatic interactions.[36] Secondly, the same biodynamers were used to form the lipophilic compartment of the DE-NPs. Finally, PNCs and DE-NPs were compared in terms of stability of NPs, EE% and LC%, and cellular uptake efficiency to provide an insight into protein delivery potential using amphiphilic polymers.

Materials and Methods
Materials
IH and GLP-1 were provided by Sanofi-Aventis Deutschland GmbH. Fetal calf serum, trypsin, RPMI 1640 cell culture medium, and NHS-fluorescein were purchased from Thermo Fisher Scientific (Darmstadt, Germany). Resomer® RG 503 H (PLGA), RBITC, Mowiol® 4–88 LA (PVA), acetic acid, sodium acetate, OVA, f-OVA, methylthiazole tetrazolium (MTT), 4',6-diamidino-2-phenylindole (DAPI), cytotoxicity detection Kit^{PLUS} (Cat. No.04744926001), and paraformaldehyde were purchased from Sigma-Aldrich (Darmstadt, Germany). MillQ water (18.2 MΩ) was obtained from a Millipore Direct-Q purification system containing a 0.22 μm filter and was used in all experiments.

A549 cells (human lung adenocarcinoma cells), obtained from the American Type Culture Collection, were cultured at 37°C in a 5% CO_2 incubator supplemented with a complete RPMI 1640 medium (containing 10% fetal calf serum).

Synthesis of Biodynamers and RBITC-Labeled OVA (r-OVA)
The synthetic protocols for amino acid hydrazides, HG-CA, and biodynamers were adopted from our previous reports.[19,24] Positively charged R-hydrazide and negatively charged E-hydrazide were included in this study to evaluate the charge influence on particle formulation based on electrostatic interaction. To synthesize R-biodynamer and E-biodynamer, R-hydrazide, or E-hydrazide and HG-CA were mixed at 1:1 molar ratio in D_2O in a final concentration of 10 mM, the addition of d-acetic acid adjusted the pD of the solution to be pD 5. After 96 h at room temperature, ^{1}H-NMR was used to confirm the polymerization.

F-hydrazide was introduced to increase the hydrophobicity of the biodynamers. Thus, RF-biodynamer was synthesized in a similar way as the above method. R-hydrazide, F-hydrazide, and HG-CA were mixed at a 1: 1: 2 molar ratio in D_2O at pD 5 in a final concentration of 10 mM. After 96 h, the polymerization was confirmed by observing aldehyde-peak depletion. The D_H of biodynamers was measured by DLS before forming particles.

r-OVA was prepared according to a modified version of a literature procedure.[37] OVA was dissolved into 0.1 M sodium carbonate solution to form a 10 mg/mL protein solution. RBITC was prepared in DMSO at 2 mg/mL, respectively. The RBITC was then added slowly into the OVA solution at a 0.25:1 ratio (RBITC: OVA, mole: mole) followed by stirring for 12 h in the dark. After that, the compounds were freeze-dried and dialyzed in DI water in the dark for 2 days.

Preparation and Physico-Chemical Characterization of NPs
Preparation of PNCs
OVA-, f-OVA- (or r-OVA-) Loaded PNCs
To prepare the PNCs, 3 μL (20 μg) of 10 mM R-biodynamer was added to 200 μL DI water. Then, OVA (10 mg/mL, in DI water) (or f-OVA, or r-OVA) was added to the R-biodynamer solution based on the weight ratio. The volume of OVA (or f-OVA, or r-OVA) utilized was minimized, resulting in a final concentration of approximately 100 μg/mL of R-biodynamer. The resulting mixture was mixed gently using a pipette. D_H (z-average) and zeta potential were measured using a Zetasizer Nano (Malvern Instrument, Malvern, United Kingdom).

IH-Loaded PNCs
IH was dissolved in 10 mM of pH 7.4 PB at 1 mg/mL due to poor water solubility in DI water. Positively charged R-biodynamer was used for negatively charged IH (1 mg/mL) in 10 mM pH 7.4 PB. The weight ratio of protein to polymer was optimized. The stability of NPs was determined by measuring the D_H change after 48 h.

GLP-1 Derivative-Loaded PNCs
Negatively charged E-biodynamer was used for positively charged GLP-1 (10 mg/mL, in DI water). The weight ratio of GLP-1 to polymer was optimized. The stability of NPs was determined by measuring the D_H change after 48 h.

Preparation of DE-NPs
DE-NPs were prepared by DE method as previously described.[38] Lyophilized R-biodynamer (1 mg) was dissolved in 500 μL DCM. f-OVA or GLP-1 (1 mg/mL, in DI water), or IH (1 mg/mL in 10 mM PB) (aqueous phase) was added into DCM (organic phase) and emulsified under 30% amplitude over 30 s using a probe sonicator (Branson Sonifier Sound Enclosure, Shanghai, China). Then, 500 μL 1% PVA (w/v) (aqueous phase) was added to the above water-in-oil (W/O) emulsion. The mixture was sonicated again under 30% amplitude for 30 s. Lastly, the water-in-oil-in-water (W/O/W) emulsion was transferred into 4 mL DI water and stirred overnight gently to remove DCM. To determine the stability of NPs, D_H, and zeta potential were measured using Zetasizer Nano. The DE-NPs were centrifuged at 8000 g for 15 min (x2) and re-suspended into the water to remove extra PVA. The PLGA-incorporated DE-NPs were prepared by adding PLGA (10 μL of in DCM, weight differs by ratio) into R-biodynamer solution (organic phase).

Morphology of NPs
The morphology of the NPs was measured using a SEM (Carl Zeiss Microscopy GmbH, Jena, Germany). To enhance the electron conductivity and image quality, samples were coated with a thin gold layer using a gold sputter (Quantum Design GmbH, Darmstadt, Germany). Microscope analysis was performed with the SmartSEM.

EE% and LC%
f-OVA-NPs were prepared using the above two methods. Then, the particles were centrifuged at 8000 g for 15 min. Free f-OVA in the supernatant was calculated by measuring the fluorescence intensity of FITC at ex/em= 494/520 nm using a microplate reader (Infinite® 200 PRO, Tecan Instrument, Crailsheim, Germany). As a control, free f-OVA was centrifuged at the same condition to confirm that free f-OVA was not spun down after the centrifugation. EE% and LC% were calculated with the following equation:

$$EE(\%) = \frac{\text{Total FITC} - \text{OVA}_{(\mu g)} - \text{Free FITC} - \text{OVA}_{(\mu g)}}{\text{Total FITC} - \text{OVA}_{(\mu g)}} \times 100$$

$$LC(\%) = \frac{\text{Total FITC} - \text{OVA}_{(\mu g)} - \text{Free FITC} - \text{OVA}_{(\mu g)}}{\text{Arg} - \text{biodynamer}_{(\mu g)} + \text{Total FITC} - \text{OVA}_{(\mu g)} - \text{Free FITC} - \text{OVA}_{(\mu g)}} \times 100$$

pH-Responsive Size Change and Degradation f-OVA-Loaded NPs
To change the pH environment and determine the pH-responsive size change of NPs, the NPs were centrifuged at 4000 g for 15 min, the supernatant was removed, and the NPs were re-suspended into 10 mM pH 5.0 AB, 10 mM pH 7.4 PB, and DI water, respectively. The D_H and PDI of NPs were determined by Zetasizer Nano after 0 h and 6 h incubations in different buffers.

The degradation analysis of protein-loaded NPs involved monitoring the absorption of a biodynamer monomer (HG-CA, Mw = 502) at 350 nm following dialysis under various pH conditions according to a modified version of a literature procedure.[39] Initially, 1 mL of 100 μg/mL NPs was placed inside a dialysis bag (Spectra-Por® Float-A-Lyzer® G2) with a MWCO (molecular weight cut-off) cut-off of 3.5–5.0 kDa. These NPs were then dispersed in 20 mL of 10 mM pH 5.0 AB, 10 mM pH 7.4 PB, and DI water, respectively. At specific time intervals (0, 2, 4, 18, 24, 28, 42, 48, and 72 h), 200

µL of the released medium was sampled. To maintain a constant volume, an equal volume of fresh medium was added. The degradation of NPs under different pH conditions was monitored by measuring the UV absorption at 350 nm. All samples were stored in a freezer prior to measurement, and the experiments were conducted in triplicate.

Structural Integrity and Release Dynamics of f-OVA in NPs

The assessment of protein structure integrity within protein-loaded NPs was carried out through RP-HPLC. This involved examining the retention time of the protein, a parameter that provides distinct information pertaining to the identical protein/peptide under scrutiny. The RP column was an ACE C4 column (100 × 2.1 mm, 3 µm particles, 300 Å pores) purchased from Avantor (US, Radnor). The C4 column was equilibrated with acetonitrile (ACN) containing 0.1% trifluoroacetic acid (TFA) in the HPLC apparatus. Five microliters of the samples was loaded onto the column, and elution was carried out by modulating the concentration of solvent A (ACN containing 0.1% TFA) utilizing solvent B (water containing 0.1% TFA) as stated in Table S1. Proteins were detected at 284 nm.

In addition to assessing retention time through RP-HPLC, protein structure integrity post-release from NPs was further evaluated using SDS-PAGE. To summarize the procedure, a 4 × Laemmli sample buffer, mixed with 2-mercaptoethanol at a 9:1 volume ratio, was added to the samples at a 1:3 volume ratio. The 5 samples analyzed comprised the marker, control f-OVA, f-OVA released from the PNCs, and f-OVA released from the DE-NPs-0% PLGA and DE-NPs -10% PLGA. Subsequently, each sample underwent a 5 min heating step at 95°C. The gel tank was prepared with 1X Laemmli SDS running buffer (Serva), 20 µL of each sample was loaded into the lanes of the Mini-PROTEAN TGX stain-free gel. Electrophoresis was conducted for 40 min at 150 V, followed by visualization under UV illumination.

The investigation into the dynamic release of protein from the protein-loaded NPs was systematically conducted within simulated acidic endosomal microenvironment and neutral conditions as controls. The NPs, post-separation from the suspension, were efficiently re-suspended in 10 mM pH 5.0 AB, 10 mM pH 7.4 PB, and DI water. Subsequent to each re-suspension, supernatant and pellets were separated via centrifugation at 8000 g for 15 min at specified time intervals (1, 2, 4, 6, 18, 24, and 48 h). Quantification of the released protein concentration was accomplished by measuring its absorbance at 492 nm in the supernatant, offering a comprehensive analysis of release kinetics across the designated time points.

Biological Characterization of NPs in vitro
Toxicity Assays

A549 cells were seeded at a density of 2×10^4 cells/well in 96-well plates, incubated overnight at 37°C. One hundred microliters of NP solutions with adjusted concentration were suspended in RPMI 1640 medium (without fetal calf serum), and added into the cells containing 100 µL of the medium. After 24 h incubation, the medium was replaced by a fresh medium containing 0.5 mg/mL MTT. The medium was removed after 4 h, and 200 µL of DMSO was added. After 10 min, absorbance at 550 nm was measured using a microplate reader. Cell viability was normalized to the absorbance of non-treated cells.

One hundred microliters of co-cultured supernatant was collected for LDH assay. Cytotoxicity detection Kit^PLUS was applied by following the assay protocol provided by the supplier. Absorbance was measured at 492 nm. Cytotoxicity was analyzed as a relative percentage compared with untreated cells as a negative control group, and Triton-X treated cells as a positive control group.

$$\text{Cellular viability}(\%) = \frac{A_{Sample\ group} - A_{DMSO\ group}}{A_{Negative\ control\ group} - A_{DMSO\ group}} \times 100$$

$$\text{LDH activity}(\%) = \frac{A_{Sample\ group} - A_{Negative\ control\ group}}{A_{Positive\ control\ group} - A_{Negative\ control\ group}} \times 100$$

Cellular Uptake Assay

A549 cells were seeded on 24-well plates at a density of 1×10^5 cells/well and incubated for 24 h. The cells were washed with pre-warmed PBS twice and treated with no treatment group, free f-OVA group, PNC group, DE-NPs, and PLGA-incorporated DE-NPs, the amount of f-OVA used in each group was 10 μg/well. After 5 h, Lysotracker red (50 nM) was added and incubated with cells for another 1 h. The cells were washed twice with PBS and stained with DAPI (5 μg/mL) for 10 min after the fixation using 4% paraformaldehyde (10 min). After washing the cells twice with PBS, we observed the cellular uptake of protein-NPs using a confocal microscope (Leica TCS SP8, Leica Mikrosysteme GmbH, Wetzlar, Germany).

Statistical Analysis

All experiments were carried out in triplicate, and data were reported as mean ± SD. One-way ANOVA and Student's *t*-tests were performed to determine the statistical significance between the groups. $0.005 < p^{***} < 0.01$, $P^{**} < 0.05$ were considered significant, and $p > 0.05$ were no statistical difference (ns).

Results and Discussion
Properties of Cargos and Biodynamers

We selected three different proteins (peptides), ovalbumin (OVA), insulin human (IH), and a glucagon-like peptide-1 derivative (GLP-1) to test PNC formation using biodynamers. OVA is one of the most commonly used model cargos in protein delivery, particularly in vaccine formulation as a model antigen. It has an isoelectric point (pI) of 4.5 and –15.3 mV of surface charge in the measurement condition with a 44.3 kDa of molecular weight (Mw) (Table 1). In addition to the OVA, two dye-labeled OVA (fluorescein isothiocyanate labeled-ovalbumin (f-OVA) and rhodamine B isothiocyanate labeled-ovalbumin (r-OVA)) were included as model cargos for monitoring the systems. IH is also often used as a therapeutic cargo for diabetes. We chose IH for comparison with OVA to see the Mw impact on polyion nano-complexes (PNCs) formation. IH has a comparable charge as OVA (–16.3 mV) under pH 7.4, but the Mw is much smaller than OVA, 5.8 kDa. To confirm the impact of charges on PNCs formation, we also included GLP-1, peptide, Mw of 4.4 kDa with a positively charged surface (+8.6 mV). Table 1 summarizes the measured surface charge with Mw of selected peptides.

To form PNCs with selected peptides, we prepared three different biodynamers taking the advantages of being able to tune biodynamers towards a particular drug cargo molecule.[20] Arginine- (R-), glutamic acid- (E-), and arginine-phenylalanine- (RF-) biodynamers having different charges and hydrophobicity were polymerized from hexaethylene glycol conjugated carbazole dialdehydes (HG-CA) and each amino acid hydrazide (R-, E-, and F-hydrazide) by adapting the reported method.[19,39,40] The successful synthesis of each biodynamers was confirmed with ¹H-NMR (Figures S1 and

Table 1 Surface Charge (ζ) and Mw of Model Cargos; ζ, Hydrodynamic Diameter (D_H), and Mw of Biodynamers

Model cargos	ζ (mV)		Mw
OVA	−15.3		44.3 kDa
IH	−16.3*		5.8 kDa
GLP-1	+8.6		4.4 kDa
Biodynamers	**ζ (mV)**	**D_H (nm)**	**Mw**
R-biodynamer	+47.1	10.7	155.0 kDa±
E-biodynamer	−11.6	7.5	67.3 kDa±
RF-biodynamer	+37.5	8.5	90.5 kDa±

Note: All of the cargo was measured in DI water (10 mg/mL), except IH. *The IH was measured in 10 mM phosphate buffer (PB, 1 mg/mL) due to its solubility. ±The Mw of biodynamers was measured using static light scattering (SLS).
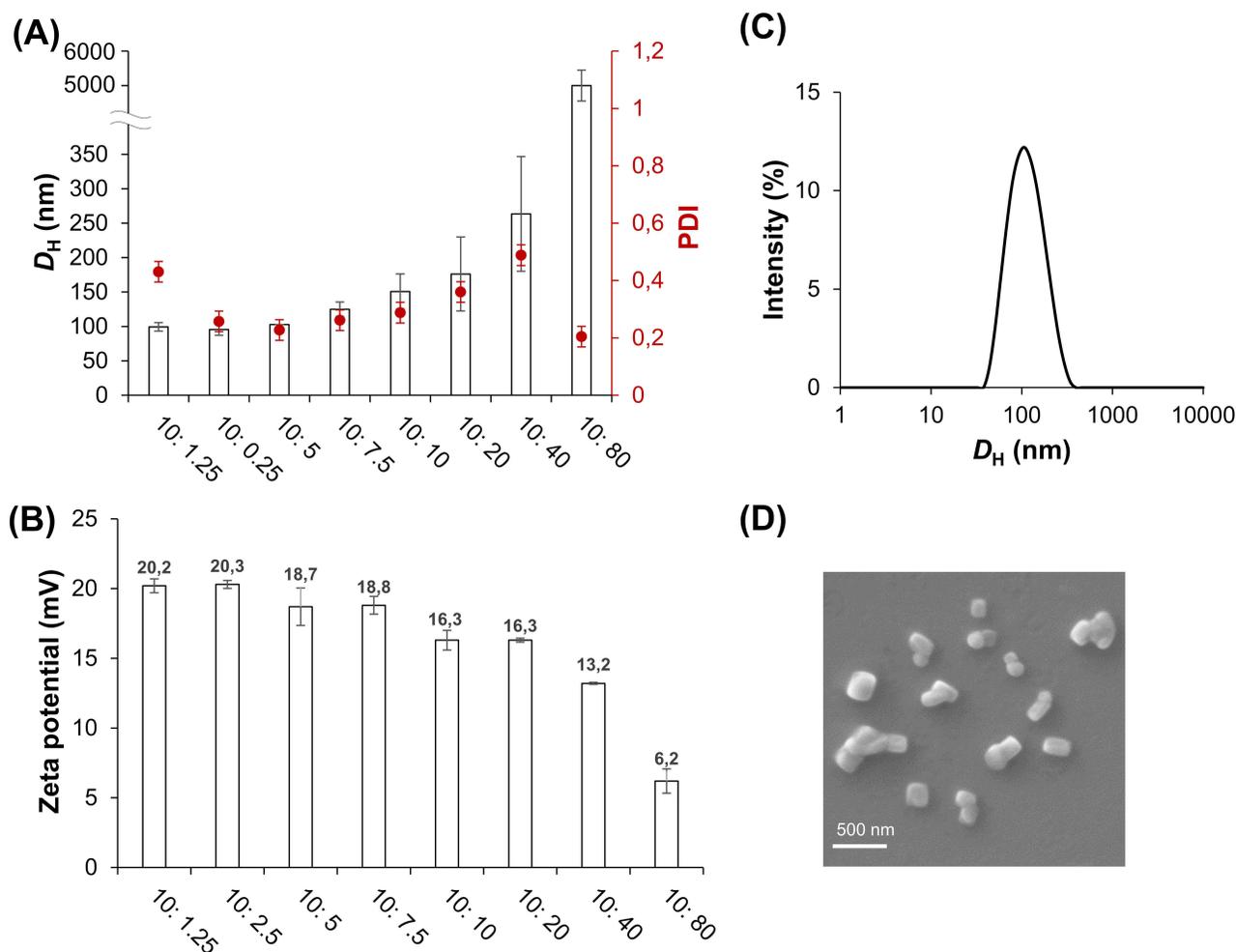
). As a positively charged biodynamer, R-biodynamer, formed with arginine residues, was prepared due to its highest protonation degree with highest pK_a among the positively charged biodynamers (histidine (H), and lysine (K)-biodynamers). The synthesized R-biodynamer was positively charged (+47.1 mV) as expected. With E residues, the E-biodynamer provided a negative surface charge of –11.6 mV. Additionally, to increase the hydrophobicity of the polymer, F-residues were included in R-biodynamers resulting in RF-biodynamers with a charge of +37.5 mV. Table 1 summarizes the surface charges and Mw of selected cargo and biodynamers.

PNCs

Formulation and Characterization of f-OVA-PNCs-R

We demonstrated PNC formation between R-biodynamer and f-OVA (f-OVA-PNCs-R), because f-OVA allows favorable quantification of the cargo after PNCs formation. Scheme 1 illustrates f-OVA-PNCs-R formation by the electrostatic interaction between oppositely charged biodynamers and cargos (R-biodynamers and f-OVA). The formed PNCs varied in hydrodynamic diameter (D_H) by weight ratios between the blended biodynamers and f-OVA. As depicted in Figure 1A, the D_H of f-OVA-PNCs-R exhibited an increment from 100 to 300 nm across the range of R-biodynamer to f-OVA weight ratios spanning from 10:1.25 to 10:80. However, an aggregation phenomenon was observed when the weight ratio of f-OVA exceeded that of R-biodynamer eightfold. Notably, the zeta potential of the PNCs displayed a declining trend as the ratio of f-OVA increased, owing to the neutralization of the positive charge conferred by R-biodynamer, as illustrated in Figure 1B. Therefore, f-OVA-PNCs-R with a weight ratio of 10:5, characterized by a D_H of 103 nm (polydispersity index (PDI) of 0.22) and zeta potential of +18.7 mV, were selected for further investigations (Figure 1C).

The morphology of the optimized f-OVA-PNCs-R was investigated using scanning electron microscope (SEM) measurements (Figure 1D). The diameter of the PNCs estimated from the SEM image fell within the range of 80 to 159 nm, which is consistent with the findings obtained from DLS measurements. An interesting finding from the SEM measurement is that the PNCs showed cylindrical shape. Composition and geometrical complexity have critical effects on self-assembled nanostructures. For example, the volume ratio between the hydrophilic/hydrophobic compartment is one crucial parameter in NP structure, increasing the hydrophobic volume ratio results in the structure change from spherical micelle, cylinder, vesicle, and membrane.[41] The underlying theory considers the nanorod structure of the R-biodynamer to be surrounded by short ethylene glycol chains, which leads to an enhanced interior (hydrophobic) volume and yields cylinders when assembled with protein. Another hypothesis is that the rod shape of biodynamers formed a layered cylindrical structure decorating f-OVA due to the electrostatic interaction between OVA and biodynamer side chains and π-π stacking between the FITC and carbazole core. To investigate the local structure of the formed cylinder PNCs, further investigation is necessary. Such a cylindrical structure is known to be advantageous over spherical nanoparticles (NPs) as it results in longer circulation times, and enhanced cellular uptake.[42] Additionally, cylinders demonstrated higher drug-loading ability over traditional spherical nano-objects.[43]

Scheme 1 Formation of PNCs through electrostatic Interaction between R-biodynamer and f-OVA.

Figure 1 D_H (left y-axis) and PDI (right y-axis) of f-OVA-PNCs at different weight ratio. White bar is D_H and red dot is PDI (**A**). Zeta potential of f-OVA-PNCs at different weight ratios (**B**). Size distribution of f-OVA-PNCs at 10: 5 (w/w), measured by DLS (**C**). Morphology of f-OVA-PNCs at 10: 5 (w/w), measured by SEM (**D**).

Drug Loading Ability and Stability of f-OVA-PNCs-R

Encapsulation efficiency (EE%) and drug loading capacity (LC%) in the delivery carrier are critically important parameters because they are directly related to the bioavailability of the drug and costs. However, most of the current NP-based protein carriers show limited protein or peptide loading ability and even lower with water-soluble peptide loading.[44] In this regard, f-OVA-PNCs-R demonstrated their excellent LC% both EE% and LE%. Figure 2A depicts that the EE% of optimized PNCs (10: 5, w/w) was 69.2%, and increased with an increasing f-OVA weight ratio. The incorporation of proteins into PNCs increased within 1:4 weight ratio, which showed the maximum EE% at 1:4 weight ratio (EE% = 88.7%, LC% = 78.0%). Also, LC% of PNCs with 10:5 weight ratio was 25.7%, which is very close to the respective theoretical maximum loading rate (33.3%). The cylindrical shape endowed large surface areas and increased inner volume of f-OVA-PNCs-R compared to conventional spherical NPs, representing excellent features for surface adsorption and drug encapsulation.[42]

Dispersion stability is one of the key physicochemical properties of NPs to assess quality, safety, and efficacy in research, especially in the preclinical phase.[43] The colloidal stability of the optimized PNCs was assessed by monitoring their size distribution over time (0, 24, and 48 h) using DLS. As can be seen in Figure 2B, the size distribution and D_H of PNCs was maintained for 48 h in DI water under neutral pH.

Protein Modification Effect in PNCs

We successfully confirmed PNC formation with f-OVA and proved their pH-responsive degradability under acidic conditions. However, we should not neglect the impact of the conjugated FITC on the cargo, as the cargo characteristics highly affect PNC formation. Thus, we have confirmed PNC formulation with OVA but without FITC-labeling. The

(A)

(B)
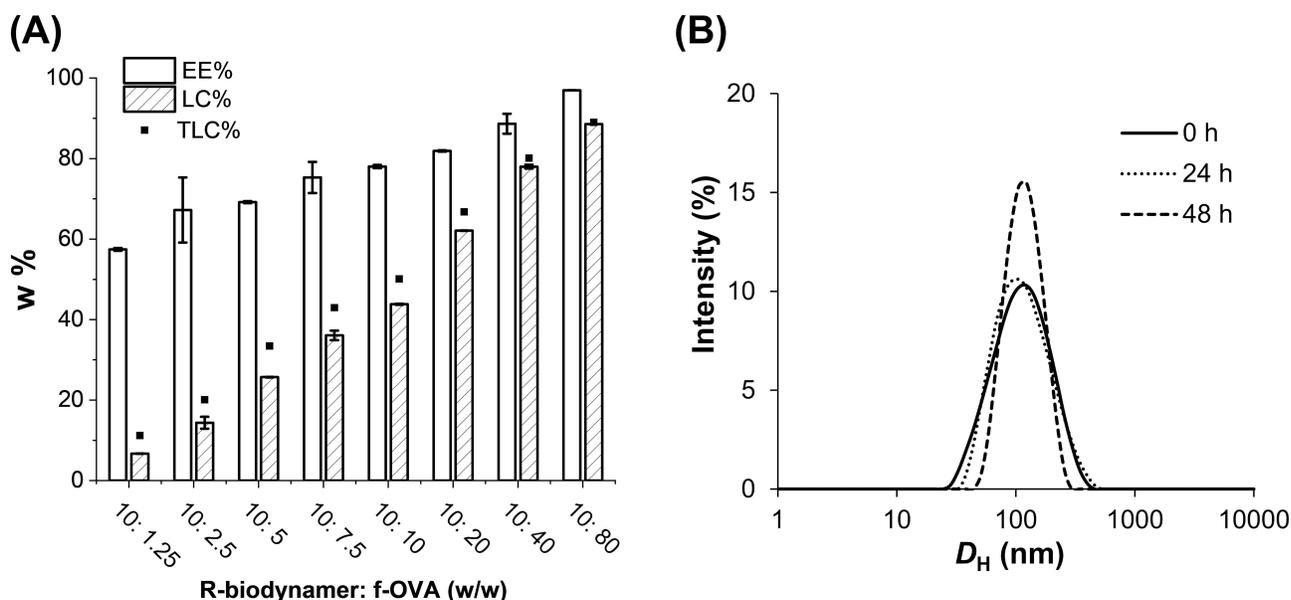
Figure 2 EE%, LC%, and theoretical loading capacity (TLC%) of f-OVA-PNCs at different weight ratios (**A**). Physical stability of 100 μg/mL f-OVA-PNCs (10: 5, w/w) for 48 h (**B**).

surface charge of unlabeled OVA was 2.3 times lower than f-OVA (Table S2), OVA successfully formed PNCs with R-biodynamer (OVA-PNCs-R) as well, a similar tendency was shown for both of the cargos, D_H of PNCs increase with protein content increase. However, the size of the OVA-PNCs-R was 1.5 times larger with higher PDI compared to the f-OVA-PNCs-R, as depicted in Figure S3A, the size distribution of OVA-PNCs-R underwent a substantial increase within a span of 2 h. Moreover, as shown in Table 2, the D_H of OVA-PNCs-R increased from 234 to 1422 nm just within 2 h, and the PDI increased to 0.50.

Our hypothesis is that the FITC (≥7 moles of FITC per mole of OVA) moiety affected the compactness of the formed PNCs by increasing the hydrophobicity, and the f-OVA formed smaller and more stable PNCs at the same weight ratio than OVA. Moreover, the aromatic ring on the FITC can be incorporated in the nanorod core of the biodynamers by π–π interactions. Additionally, the lowered surface charge of OVA might affect the decrease in PNC stability due to the reduced electrostatic interactions in PNC formation. Such charge, hydrophobicity, and aromatic rings of the cargo affected the PNC stability.

To examine the hypothesis and the effect of dye-labeling of cargo on PNC formulation, another hydrophobic dye, rhodamine B isothiocyanate (RBITC), was introduced into the OVA (r-OVA). As depicted in Figure S3B, r-OVA-loaded R-biodynamer PNCs (r-OVA-PNCs-R) were successfully formed. They were stable in size for 48 h, similar to f-OVA-PNCs-R. Therefore, we conclude that the conjugating hydrophobic moiety like FITC and RBITC, more ideally drugs, on

Table 2 D_H, PDI, and DCR of OVA-, IH-, and GLP-1-Loaded PNCs for 2 h

PNC Components	Incubation Time (h)	D_H (nm)	PDI	DCR (kcps)
OVA-PNCs-R	0	234	0.32	6940
	2	1422	0.50	5410
IH-PNCs-R	0	356	0.33	68,655
	2	1260	0.23	54,460
GLP-1-PNCs-E	0	145	0.25	7857
	2	912	0.60	1793

the protein can be beneficial in enhancing PNC formation and stability, which may be due to the charge, hydrophobic, and π–π interactions between the cargo and the polymer.[45]

However, the modified form of the protein has a risk of reduced efficacy due to irreversible modification, and modified proteins cannot be an option depending on the protein structure. Therefore, we also tested a strategy keeping the cargo in PNCs in a stable manner by modifying the polymer. To increase the compactness and stability of unlabeled OVA-PNCs, we modified R-biodynamers to include phenylalanine monomers (F), exploiting their excellent tunability. We expected the RF-biodynamers to increase the hydrophobicity as well as π- π interactions with the carbazole core. Using the RF-biodynamers, OVA-PNCs (OVA-PNCs-RF) were successfully formed with a D_H of 116 nm (PDI = 0.23), which was close to f-OVA-PNCs-R. However, the D_H started increasing to 183 nm (PDI = 0.25) within 2 h. The D_H increase of OVA-PNCs-RF was smaller than that of OVA-PNCs-R. It suggests that the hydrophobic moiety of the polymer successfully decreased the size of PNCs and increased the stability of PNCs (Figure S3A, S3C). Therefore, we conclude that the hydrophobic modification of biodynamers improves PNC stability, although not sufficient as much as cargo modification, because an increase in the hydrophobicity of RF-biodynamers leads to a loss of charge density and electrostatic interaction by replacing R with F.

Impact of Mw and Charge of Cargos on PNCs Formation

As one of the factors that affects the dispersity and stability,[46] the Mw of the cargo needs to be considered during the formulation of PNCs. To see the impact of cargo Mw, a biologically functional peptide, IH, having 7.6 times lower Mw but comparable surface charge (–16.3 mV) with OVA (–15.3 mV), was tested in PNC formation. IH and R-biodynamers formed IH-PNCs-R of 326 nm (PDI = 0.20); however, the size increased to 1260 nm (PDI = 0.23) in 2 h of incubation (Table 2, Figure S3D) in DI water, same as for OVA-PNCs-R. As tested in OVA, the RF-biodynamer was applied to increase the stability and compactness due to increased hydrophobicity. However, as shown in Figure S3E, the increased hydrophobicity and π–π interactions in the IH-PNCs-R were not helpful as much with respect to stabilization properties. The size of the IH-PNCs-RF formed with RF-biodynamer increased rapidly in 2 h as well. IH is smaller than OVA in Mw, resulting in a reduced size of polyelectrolyte cores in PNCs, which may cause lower stability than the OVA.

The PNC formation was also tested for a positively charged GLP-1 derivative using a negatively charged biodynamer, E-biodynamer (GLP-1-PNCs-E). Similarly, the GLP-1-PNCs-E were successfully formed but had limited stability (Figure S3F). The GLP-1-PNCs-E aggregated even faster than IH-PNCs-R due to the lowered net charges with lowered Mw of the cargo.

Conclusively, regardless of the Mw, the proteins/peptides having surface charges formed PNCs with biodynamers based on the electrostatic interaction;[47] however, the surface charge affects the electrostatic repulsion/attraction between cargo and biodynamers resulting in a different range of NP sizes.[48] Augmenting the zeta potential of NP yields superior stability of the system.[49] Moreover, the stability of the resulting PNCs was also highly influenced by the hydrophobic and π–π interactions between cargo and polymer.[45] With a thorough understanding, PNC formation using biodynamers can be an excellent option for protein/peptide delivery based on their exceptionally high drug-loading efficiency compared to any other NP formulation methods currently available.[29] However, as discussed above, the chemical properties of protein/peptide affect the formulation and stability of PNCs, once protein/peptide modification is not an option, PNC formation with the current biodynamers has limitations in reaching a feasible level of stability for biological application. Therefore, it needs further strategies to develop biodynamers as protein/peptide delivery carriers, such as crosslinking or different formulation methods like the DE-method.

pH-Responsive Size Change and Degradation of f-OVA-PNCs-R

The reversible and dynamic feature of biodynamers makes the resulting f-OVA-PNCs-R pH-responsive and release cargo in an acidic environment at the target, such as extracellular environment of cancer, inflammation, infection, and intracellular environments like endosomes.[50] Therefore, we assessed the pH-responsiveness of PNCs to confirm controlled release of cargo under dynamic conditions. The f-OVA-PNCs-R were placed in different solutions, DI water, 10 mM phosphate buffer (PB) at pH 7.4, and 10 mM acetate buffer (AB) at pH 5.0, at 37°C (Figure 3A). The PNCs remained stable in D_H in DI water and pH 7.4 PB for 6 h compared to their D_H at pH 5.0 AB. The D_H of f-OVA-
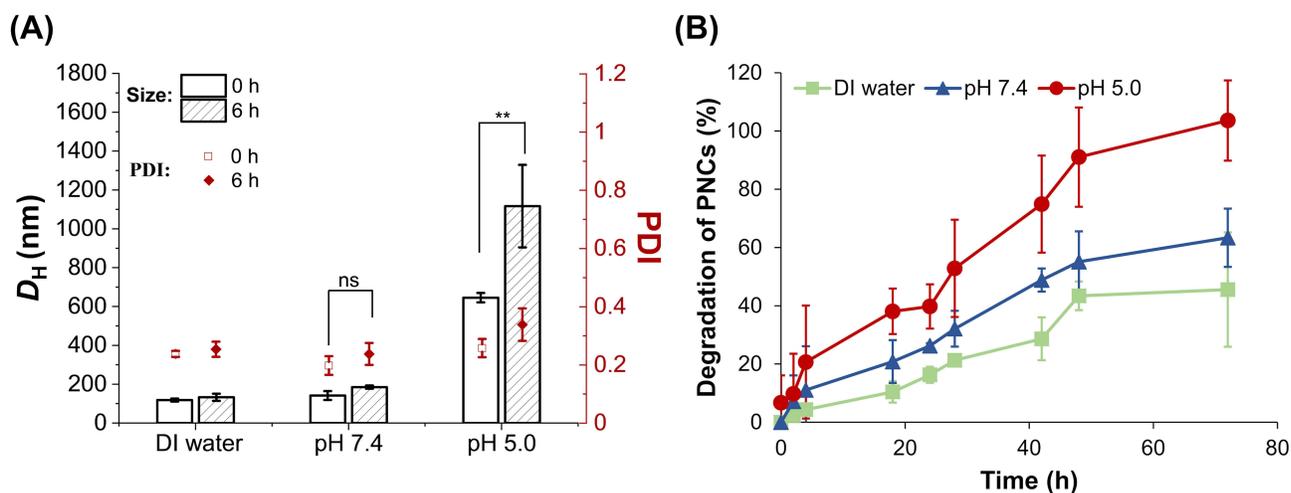
Figure 3 pH-Responsive size change of 100 µg/mL f-OVA-PNCs (10: 5, w/w) in DI water, pH 7.4 (10 mM PB), and pH 5.0 (10 mM AB) for 6 h (**A**). Acid-responsive degradation of f-OVA-PNCs (10: 5, w/w) in DI water, pH 7.4 (10 mM PB), and pH 5.0 (10 mM AB) for 48 h (**B**). The comparison of mean size changes in PNCs at 0 and 6 h under pH 7.4 and pH 5.0, respectively, was conducted using a *T*-test. P** < 0.05 was considered significant, and p[ns] > 0.05 were no statistical difference.

PNCs-R immediately increased to 645 nm at pH 5.0 and further increased to 1116 nm after 6 h. The D_H increase at pH 5.0 was attributed to the decomposition of the dynamic backbone and the continuous degradation of biodynamer led to the PNCs swelling. It was also reported that pH-responsive swelling accelerates the release of drug from the loose nanocarriers and results in burst release.[51] Conclusively, the PNCs formed by electrostatic interactions were stable at neutral pH and destabilized at acidic conditions due to the pH-responsive degradation of the incorporated biodynamers, which is in line with the expectations.

To confirm the degradation of R-biodynamer from the f-OVA-PNCs-R under dynamic conditions, we monitored monomer or oligomer (<5 kDa) release from the PNCs using UV absorbance of HG-CA at 350 nm. Note that the UV absorbances of f-OVA and amino acid monomers at 350 nm are negligible compared to HG-CA (see Figure S4). After 4 h of incubation in AB at pH 5.0, 20.7% of biodynamers were degraded into fragments smaller than 5 kDa, while 11.1% and 4.3% of biodynamers were degraded in PB at pH 7.4 and DI water, respectively. This degradation was attributed to the re-equilibration of HG-CA monomers within the biodynamer backbone during the re-suspension process. Within 72 h under the acidic condition, the biodynamers in the f-OVA-PNCs-R completely (103.6 ± 13.8%) degraded into short oligomers or monomers, which was twice as much degradation as observed at pH 7.4 and in DI water (63.3 ± 10.0% and 45.6 ± 19.6% degradation, respectively) (Figure 3B). The results support that the swelling of the f-OVA-PNCs-R at pH 5.0 is attributed to the degradation of biodynamers.

Double Emulsion Nanoparticles (DE-NPs)
Formulation and Characterization of f-OVA-DE-NPs-R

Unlike the PNC formation, the charge of polymer and cargo affects DE-NPs formation less, which means that this formulation method does not necessarily require a specific polymer design for each cargo.[52] Also, the stability of DE-NPs is known to rely more on the polymers and emulsifiers used and less on the cargos,[12] which is different from our observation for PNCs. Therefore, we demonstrated DE-NPs formation using R-biodynamers and compared it with PNCs particularly in colloidal stability.

Scheme 2 illustrates formation methods of DE-NPs. Biodynamer in "oil"-phase (0.5–2 mg/mL, 0.5 mL of dichloromethane (DCM) and protein in water-phase (0.5–1 mg/mL, 0.1 mL of DI water) were completely emulsified in the first emulsification and followed by the second emulsification step with 1% polyvinyl alcohol (PVA) (aq). The formation was tested with three different cargo weight ratios against added R-biodynamers. As a result, DE-NPs were formed with a D_H range of 166–283 nm (PDI: 0.28–0.46) by cargo weight ratios. The D_H and PDI became reduced with decrease of f-OVA content from 30% to 10% (against biodynamer, weight ratio). Also, 10% f-OVA formed a greater number of NPs, which
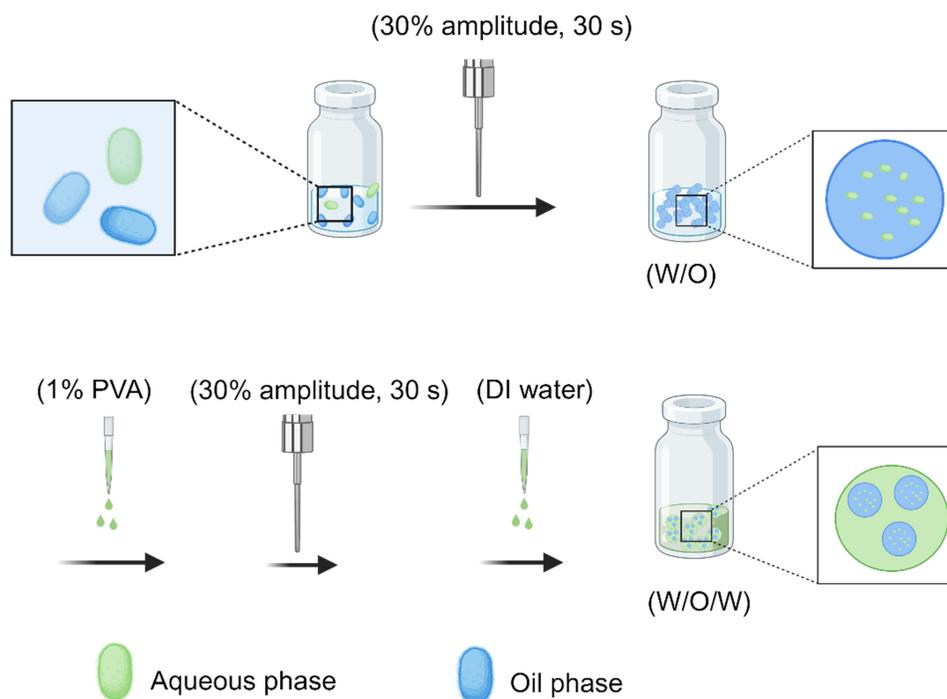
Scheme 2 Preparation of Protein-loaded DE-NPs via DE method.

resulted in a higher number of derived count rate (DCR) even with smaller NP size in the DLS measurements. DCR is the value related to the scattered photon in the measurements, thus, increasing with increased particle numbers or increased particle size. In terms of the zeta potential, all DE-NPs had a slightly positive electric charge, and showed no significant differences by cargo ratio (Table 3). From these results, we concluded that the 10:1 weight ratio of R-biodynamers and f-OVA generated monodispersed NPs with the highest efficiency and can be seen as an optimized condition for the following investigations. The resulting f-OVA-DE-NPs exhibited excellent dispersion in an aqueous solution (Figure 4A) and spherical morphology (Figure 4B, measured by SEM).

As one of the most important physicochemical properties of NPs, shape is an important design parameter for drug carriers and plays a multifaceted role in particle adhesion, distribution, and cell internalization.[53] Non-spherical particles possess a theoretically higher area of surface-adhesive interactions than spherical particles.[54] It is demonstrated that shape affects phagocytosis in cell–particle interactions.[55] Spherical shapes demonstrated enhanced cellular uptake compared to cylindrical particles, owing to the smaller dimensions of early endocytic vesicles relative to cylindrical counterparts, which necessitates additional energy for the internalization of cylindrical particles.[56] The comprehensive understanding of particle shape as a design parameter for practical medical applications remains limited, additional pivotal experiments such as quality control measures are crucial as well to bridge the gap between particle design to practical utility.[57]

Table 3 D_H (SD $\leq \pm$ 50), PDI (SD $\leq \pm$ 0.05), ζ (SD $\leq \pm$ 0.7), and DCR (SD $\leq \pm$ 3000) of f-OVA-DE-NPs

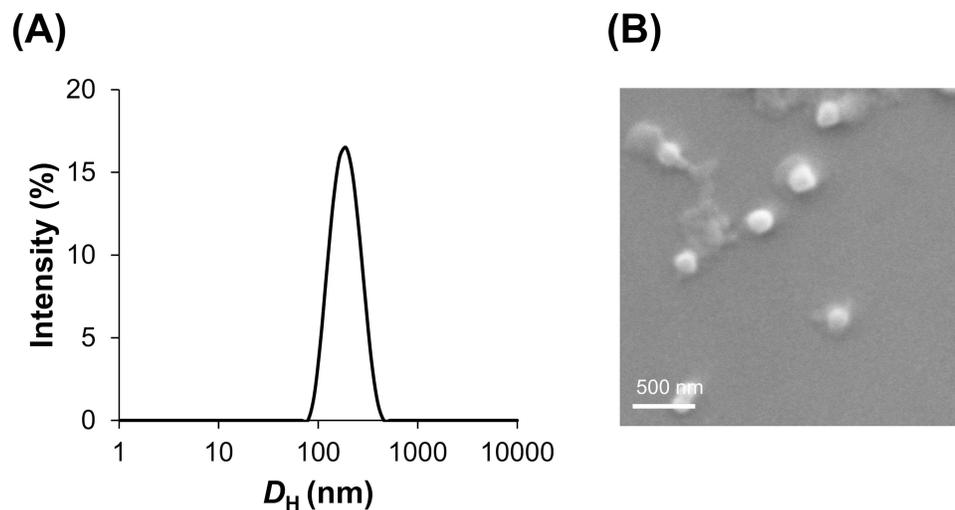| f-OVA-DE-NPs	D_H (nm)	PDI	ζ (mV)	DCR (kcps)
10% f-OVA	166	0.28	+4.8	18345
20% f-OVA	268	0.29	+4.7	9001
30% f-OVA	283	0.46	+4.4	4297

(A)

(B)

Figure 4 Size distribution of DE-NPs (R-biodynamer: f-OVA, 10: 1, w/w) in aqueous solution (**A**). Morphology of DE-NPs (R-biodynamer: f-OVA, 10: 1, w/w), measured by SEM (**B**).

Drug Loading Ability and Stability of f-OVA-DE-NPs-R

We assessed the EE% and LC% of the DE-NPs and compared them with the PNC formation method. As depicted in Figure 5A, a notable increase in EE% and LC% was observed with an increase in the amount of PLGA used. This may align with PLGA which contributed to the enhanced stability of the protein within the particles. However, the EE% and LC% of f-OVA-DE-NPs-0% PLGA (EE%=20.6, LC%=1.9%) and f-OVA-DE-NPs-10% PLGA (EE%=32.8%, LC=2.9%) were significantly lower compared to those of f-OVA-PNCs-R (EE%=69.2%, LC%=25.7%). Particularly, low LC% of DE-NPs, less than 5%, is one typical challenge in NP formulation using emulsification methods.[58–60]

The size distribution of the f-OVA-DE-NPs-R (10:1, w/w) were monitored for 48 h. Figure 5B and 5C depict the stable maintenance of the D_H of DE-NPs in DI water during this timeframe. The stability of the DE-NPs was also evaluated in Hank's Balanced Salt Solution (HBSS), a saline solution commonly employed for maintaining optimal osmotic pressure and physiological pH in the cell culture. Figure S5A illustrates the sustained size distribution of DE-NPs in HBSS, showcasing stability even as the D_H increased over time (302 nm, PDI=0.43). Notably, the derived count rate (DCR) exhibited a significant decrease from 10,686 to 2413 kcps within a 12 h period. It is worth mentioning that, under this condition, PNCs dissociated immediately. While the stability of DE-NPs surpasses that of PNCs, further enhancement is imperative to facilitate subsequent in vitro and in vivo investigations.

(A)

(B)

(C)
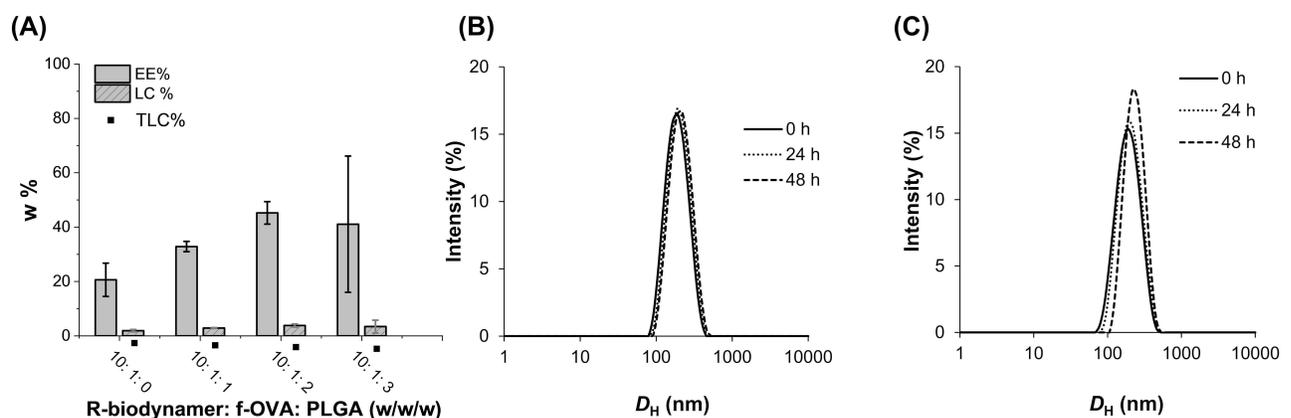
Figure 5 EE%, LC% and TLC% of f-OVA loaded DE-NPs with various amounts of PLGA (R-biodynamer: f-OVA: PLGA, 10: 1: x, w/w/w) (**A**). Stability of f-OVA-DE-NPs-0% PLGA (**B**) and f-OVA-DE-NPs-10% PLGA (**C**) in DI water for 48 h.

PLGA is extensively tested in DE-NP formation for protein delivery, owing to its versatility in formulation and biocompatibility.[61] In this context, PLGA (10%, 20%, and 30% against biodynamer, weight ratio) was incorporated in the formulation to further stabilize the DE-NPs. As shown in Table S3, the addition of 10% PLGA showed the lowest PDI with the highest DCR (19,385 kcps), which suggests the formation of more monodispersed DE-NPs with higher efficiency. Thus, DE-NPs with 10% PLGA (10:1: 1, w/w/w) were utilized for further studies as a comparison with DE-NPs without PLGA (10:1: 0, w/w/w). As shown in Figure S5B, DE-NPs-10% PLGA demonstrated a consistent size distribution with a D_H of 230 nm (PDI=0.30) for 12 h, accompanied by a slight decline in DCR value (from 13,655 to 10,459 kcps) in HBSS. These results indicate that the incorporation of PLGA significantly enhances the stability of DE-NPs under physiological conditions.

Impact of Cargos on DE-NPs Formation

OVA, IH, and GLP-1 were encapsulated within DE-NPs utilizing R-biodynamer. Figure S6 illustrates the D_H distribution of emulsions loading OVA, IH, and GLP-1, both with and without PLGA. The DE-NPs incorporating PLGA exhibited a slightly smaller D_H compared to those without PLGA, aligning with the trend observed for f-OVA-DE-NPs (Figure S6A). This reduction in D_H can be attributed to the ability of PLGA to form smaller droplets, which rapidly absorb at the water–oil interface, consequently enhancing the stability of the emulsion system.[62] As can be seen in Figure S6C, positively charged GLP-1 did not influence DE-NP formation of positively charged R-biodynamer. The stability of DE-NPs loading OVA, IH, and GLP-1 was thoroughly examined. As presented in Table 4, the D_H of DE-NPs remained constant over a period of 48 h, indicating excellent stability. This highlights a distinct advantage of DE-NPs over the PNC formation method, as the characteristics of the cargo molecules had minimal impact on the formation of DE-NPs. Consequently, DE-NPs possess considerable potential for delivering diverse proteins or peptides utilizing a unified formulation approach. However, it is noteworthy that PNCs exhibited a higher LC% compared to DE-NPs, as evident from the results.

pH-Responsive Size Change and Degradation of DE-NPs

To confirm the pH-responsiveness of the DE-NPs, the size change and degradation of DE-NPs were determined under different pH conditions. DE-NPs were washed twice with DI water to remove excess PVA and placed in DI water, PB at pH 7.4 and AB at pH 5.0. During the washing process, a slight aggregation of the NPs occurred, resulting in an increase in the size of the DE-NPs from 150 to 300 nm. As shown in Figure 6A, the D_H of the DE-NPs increased negligibly in DI water and 10 mM pH 7.4 PB within 6 h (remained 300–350 nm of D_H, and 0.20 – 0.30 of PDI). However, the D_H increased significantly to 750–800 nm in 10 mM pH 5.0 AB immediately, and its PDI also drastically increased from 0.20 to 0.60. Therefore, DE-NPs maintained the pH-responsive ability of biodynamer and swelled and aggregated under an acidic environment.

The acid-responsive degradability of DE-NPs was investigated using the dialysis bag diffusion method. The results depicting the percentage degradation of f-OVA-DE-NPs are presented in Figure 6B (DE-NPs-0% PLGA) and Figure 6C (DE-NPs-10% PLGA). Within the initial 4 h under pH 5.0, approximately 10% degradation was observed for both DE-NPs-0% PLGA and DE-NPs-10% PLGA. However, no significant degradation occurred during the 4 h period in DI water and pH 7.4 for both DE-NPs. Over the following three days, DE-NPs-0% PLGA exhibited more rapid degradation than DE-NPs-10% PLGA at pH 5. Specifically, the degradation values reached 52.3% and 34.1% at 72 h, respectively. This disparity in degradation rates can be attributed to the influence of PLGA on the stability of DE-NPs. The PLGA provides

Table 4 D_H and PDI of OVA (or Insulin, or GLP-1)-DE-NPs-R Measured After 48 h at R.t

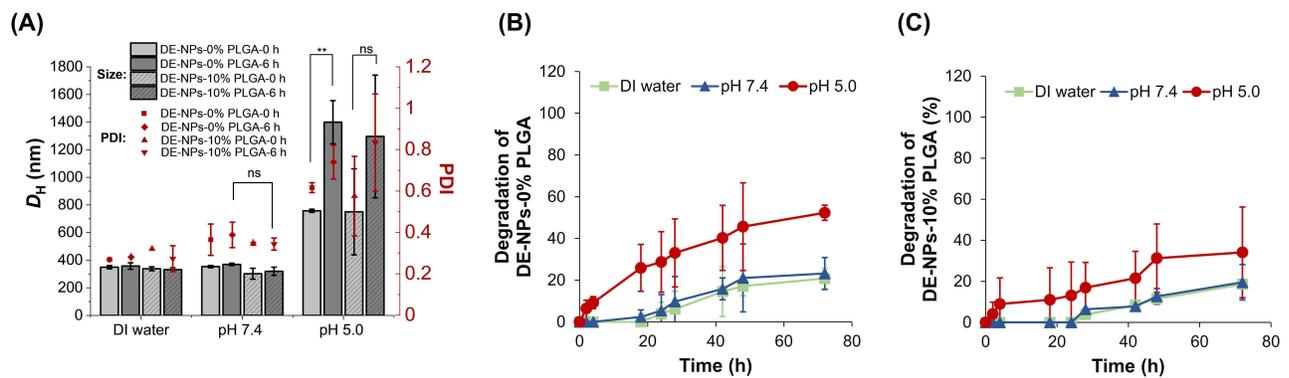|	With X% PLGA	D_H (nm)	PDI
OVA-DE-NPs-R	0%	214 ± 49	0.48 ± 0.11
	10%	189± 48	0.26 ± 0.02
IH-DE-NPs-R	0%	200 ± 11	0.45 ± 0.07
	10%	183± 34	0.30 ± 0.09
GLP-1-DE-NPs-R	0%	199 ± 9	0.3 ± 0.09
	10%	189± 62	0.30 ± 0.02

Figure 6 pH-responsive size change of 100 µg/mL f-OVA-DE-NPs-0% PLGA and DE-NPs-10% PLGA in DI water, pH 7.4 (10 mM PB), and pH 5.0 (10 mM AB) for 6 h (**A**). Acid-responsive degradation of f-OVA-DE-NPs-0% PLGA (**B**) and DE-NPs-10% PLGA (**C**) in DI water, pH 7.4 (10 mM PB), and pH 5.0 (10 mM AB) for 48 h. The comparison of mean size changes in PNCs at 0 and 6 h under pH 7.4 and pH 5.0, respectively, was conducted using a T-test. $P^{**} < 0.05$ was considered significant, and $p^{ns} > 0.05$ were no statistical difference.

protection, rendering the biodynamer resistant to acidic conditions. Sustained degradation of DE-NPs was observed in DI water and pH 7.4 buffer solution, akin to the PNCs.

Structural Integrity and Release Dynamics of f-OVA in NPs

Post-encapsulation, the preservation of protein activity is of paramount importance. Therefore, reversed-phase high-performance liquid chromatography (RP-HPLC) was employed to scrutinize the retention time of the encapsulated f-OVA subsequent to its release from the NPs. As depicted in Figure S7A–S7D, the retention time of all f-OVA instances remained consistent, affirming the identical chemical structure of f-OVA both post-encapsulation and subsequent release from the NPs. This finding aligns seamlessly with prior studies that have independently confirmed the sustained activity of the protein following encapsulation.[63] Additionally, the integrity of the protein/peptide structure following encapsulation and release from PNCs, DE-NPs-0% PLGA, and DE-NPs-10% PLGA was corroborated through sodium dodecyl sulfate-polyacrylamide gel electrophoresis (SDS-PAGE) analysis, as illustrated in Figure S7E. Notably, the observed band positions were consistent across all three formulations, further validating the preservation of structural integrity during the encapsulation and release processes from both kinds of PNCs and DE-NPs.

Following the successful liberation of f-OVA, the acid-triggered degradation of PNCs facilitated this process. As depicted in Figure S4, the substantial absorbance at 492 nm exhibited by f-OVA was attributed to the FITC labeling. Therefore, we monitored f-OVA release from the NPs using their absorbance at 492 nm. Noteworthy to mention that R-biodynamer and the biodynamer-degraded monomer demonstrated no absorbance at this wavelength. As shown in Figure 7A, the PNCs exhibited a remarkable release efficiency, discharging 95.0 ± 16.5% of f-OVA under acidic condition within 6 h, while 38.0 ± 1.0% of the f-OVA released under neutral conditions (pH 7.4). Significantly

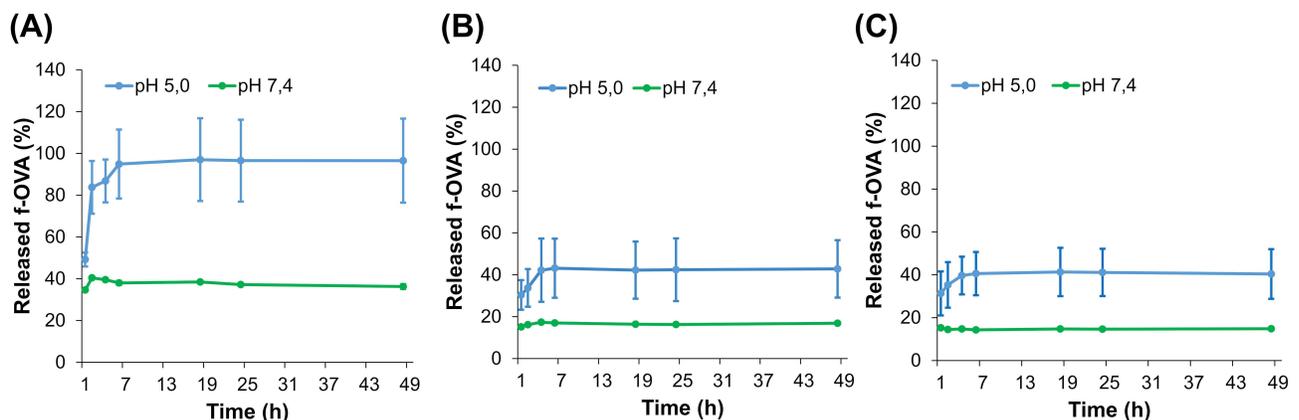**Figure 7** Release dynamic f-OVA in PNCs (**A**), DE-NPs-0% PLGA (**B**), and DE-NPs-10% PLGA (**C**) in pH 5.0 (10 mM acetate buffer) and pH 7.4 (10 mM PB)₂.

accelerated cargo release under the acidic condition affirms the controlled release of the protein encapsulated within PNCs but with a substantial leakage under the neutral condition due to the inherent instability of the PNCs.

As shown in Figure 7B and 7C, the DE-NPs-0% PLGA formulation exhibited a release profile of 30.4 ± 7.1% of f-OVA at pH 5.0 within 1 h, with a release rate to 42.8 ± 13.7% after 48 h. Remarkably, DE-NPs-10% PLGA demonstrated an expedited release, with 31.3 ± 10.3% of f-OVA released within 1 h under acidic conditions. Furthermore, at the same time point, DE-NPs-10% PLGA released 40.4 ± 11.6% of f-OVA, a release pattern that exhibited no statistically significant difference when compared to DE-NPs-0% PLGA. However, this release was notably lower than that observed with PNCs. These outcomes substantiate the efficacy of the DE method in ensuring the stable loading of proteins within NPs. Notwithstanding the stability exhibited by DE-NPs, they remain responsive to acidic pH, facilitating the release of protein cargo through the degradation of biodynamers. Consequently, these findings alleviate conventional concerns associated with the restricted cargo release from DE-NPs, albeit still indicative of a slower release compared to PNCs.

DE-NPs and PNCs exhibit analogous characteristics concerning pH-responsive D_H changes and degradation. Through a comparison of the degradation and release data, it is evident that PNCs demonstrate a more rapid pH-responsive behavior compared to DE-NPs, which is attributed to a variety of physical, chemical, and processing factors such as the homogeneous drug distribution, polymer morphology, and composition.[64] Furthermore, it is noteworthy that PLGA may impede the diffusion of DE-NPs, thereby contributing to the decelerated pH-responsive degradation of the biodynamer.[65] The rapid pH-responsive behavior induced the fast release of protein/peptide represents an important phenomenon in drug delivery.[64] On the other hand, DE-NPs exhibit greater stability than PNCs in pH 7.4 buffer solution. Notably, DE-NPs benefit from additional protection offered by PLGA, further enhancing their stability in these environments.

Biocompatibility and Cellular Uptake of PNCs and DE-NPs

A549, a widely employed human lung cell line, stands as a preeminent choice for investigating interactions between particles and cells, and it has proven efficacy in elucidating diverse aspects such as cytotoxicity, transport, oxidative stress, and inflammatory responses in the context of acute exposures ranging from 24 to 72 h to various materials.[66,67] Therefore, the cell viability of PNCs and DE-NPs was evaluated with A549 cells using MTT method and lactate dehydrogenase (LDH) assays by measuring the mitochondrial dehydrogenase activity and LDH, respectively.[68] As shown in Figure 8, PNCs and DE-NPs all showed negligible influence in cell viability (above 90%) even at the tested highest concentration (100 μg/mL). The cytotoxicity measured by LDH assay was close to 0%, which was consistent with MTT results. Therefore, the formulation methods using the same biodynamers showed similar biocompatibility and
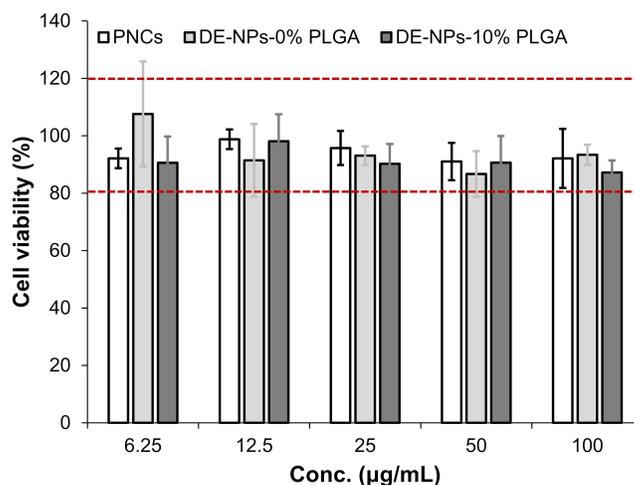

Figure 8 Cell viability of f-OVA-loaded NPs on A549 cells analyzed by MTT assay. White bar is f-OVA-PNCs-R (10: 5, w/w); light gray bar is f-OVA-DE-NPs-0% PLGA; dark gray bar is f-OVA-DE-NPs-10% PLGA. (n=6). A one-way ANOVA was employed to assess the statistical differences in cell viability among PNCs, DE-NPs-0% PLGA, and DE-NPs-10% PLGA. The red lines represent the standard values of the control group.

cellular viability, and both PNCs and DE-NPs are biocompatible at below 100 μg/mL with the mammalian cells, which enabled therapeutic application in vitro and in vivo.

The cellular internalization of PNCs and DE-NPs was compared through a comprehensive experimental setup. No treatment control, free f-OVA, f-OVA-PNCs (10:5, w/w), f-OVA-DE-NPs-0% PLGA, and f-OVA-DE-NPs-10% PLGA were incubated with A549 cells for 6 h. Figure 9 visually demonstrates the results of the experiment. For a better comparison, the mean fluorescence intensity (MFI) of f-OVA obtained in Figure 9 was quantified using Image J software (Figure S8). The fluorescence from lysosome (labeled by LysoTracker Red) and f-OVA indicates that both types of NPs exhibit higher cellular uptake compared to free f-OVA. The PNCs exhibited the highest MFI (168.8 a.u.) among the NPs, 1.5-fold higher than that of DE-NPs. However, the concentrated and vibrant green fluorescence observed in the case of f-OVA-PNCs can primarily be attributed to the aggregation of positively charged NPs around the negatively charged cell membrane, as previously reported rather than the cell internalization. On the other hand, the overlapping red and green
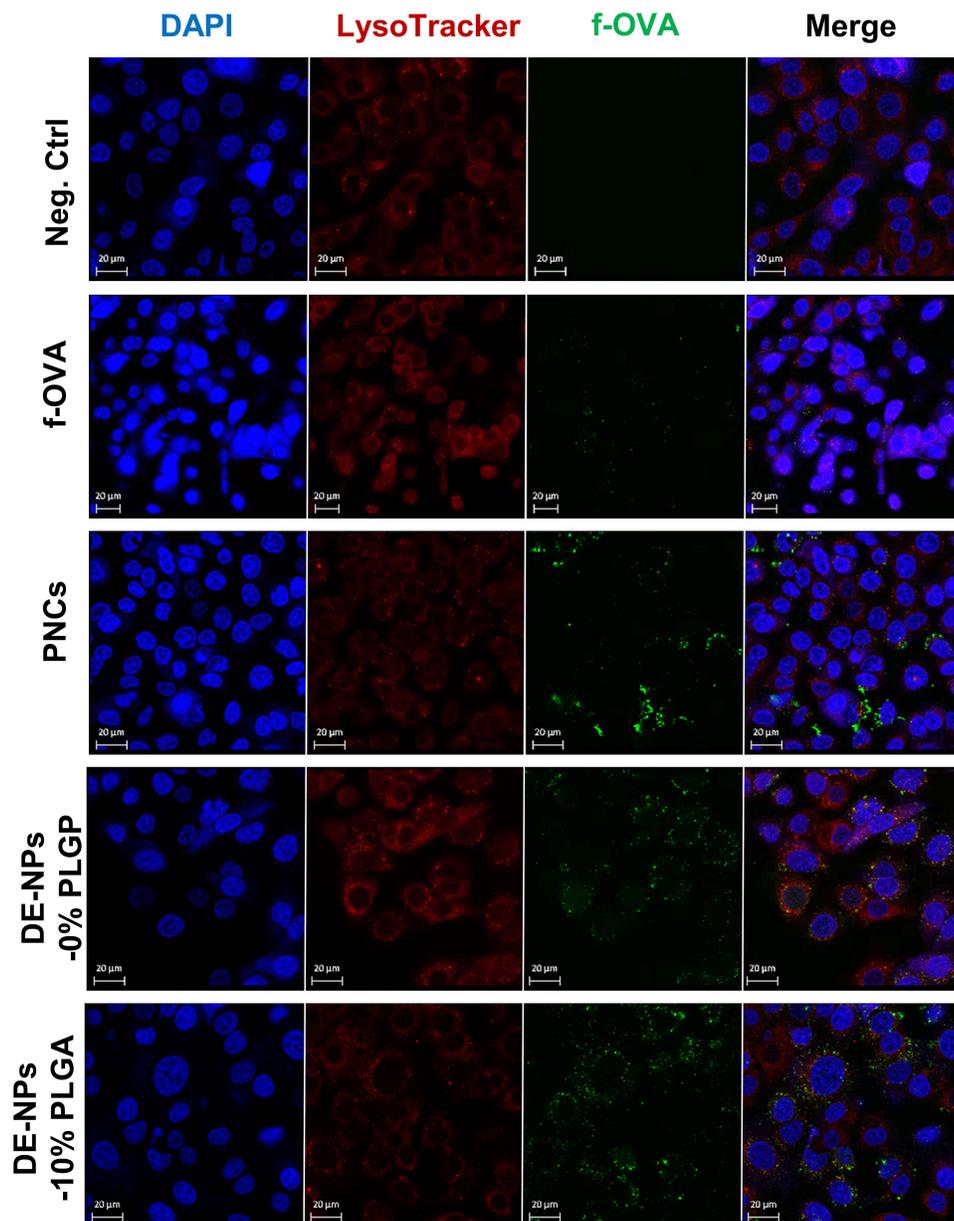

Figure 9 A549 cellular uptake of f-OVA-loaded NPs after 6 h incubation. DAPI stained nucleus in blue, LysoTracker™ Red DND-99 stained endosome/lysosome in red, and f-OVA in green.

fluorescence in DE-NPs-0% PLGA and DE-NPs-10% PLGA showcases the well-distributed presence of DE-NPs within the cells, which can be attributed to the improved stability of these NPs compared to PNCs. Notably, the incorporation of 10% PLGA augmented the cellular uptake of DE-NPs in comparison to DE-NPs-0% PLGA, resulting in respective MFI of 125.1 a.u. and 112.3 a.u. Conclusively, PNCs showed high cellular uptake potential compared to DE-NPs due to the affinity with cell membranes; however, with more physiological stability, DE-NPs exhibit more uniform dispersion than PNCs.

Biomedical Applications of PNCs and DE-NPs

Polymeric NPs enable delivery of various cargos including small molecules, biological macromolecules, proteins, and vaccines.[60] Our biodynamers establish resilient pathways for protein delivery through the formation of PNCs and DE-NPs. The utilization of biodynamers not only amplifies the stability of protein drugs but also expedites their cellular uptake and facilitates precise cytosolic release.

Physiological microenvironments with acidic conditions can serve as valuable biomarkers for various diseases, offering dual functionality as both treatment targets and diagnostic indicators.[69] pH-Responsive drug delivery systems have emerged as a prominent modality in various medical domains, such as cancer diagnosis and treatment,[70] diabetes therapy,[71] skin disease therapy,[72] and anti-bacterial applications.[73] Peptide-loading PNCs formed with biodynamers offered enhanced efficacy and reduced systemic toxicity, attributable to their high drug LC% and controlled-release capabilities triggered by changes in pH.[74] Additionally, in our investigation, DE-NPs formed using the same biodynamers exhibited exceptional monodispersity and elevated stability. Moreover, our study underscored the consistent preservation of the pH-responsiveness inherent in DE-NPs. The promising attributes of our PNCs and DE-NPs suggest their significant potential in advancing the field of drug delivery.

However, prospective research is crucial to evaluate the scalability, stability, and in vivo behavior of both PNCs and DE-NPs. When comparing particle formation methods, protein delivery efficiency assessed by delivered protein functions is the critical aspect. However, given the challenges of evaluating the model protein and peptide drug efficacy using in vitro assays and the varied conditions encountered in vivo (e.g., high serum protein concentration, biological barriers like mucus, and biochemical interactions), such comparisons should be conducted in future in vivo studies. These critical investigations will contribute to a comprehensive understanding of the translational viability and broader implications of these delivery systems.

Conclusions

This study aimed to explore the potential of pH-responsive amphiphilic biodynamers as innovative materials for protein delivery, manifesting within PNCs and DE-NPs. Particularly, our focus was on a comparative analysis of the distinctive attributes exhibited by PNCs and DE-NPs, both formulated utilizing the same biodynamer. Evidently, the loading efficiency of PNCs surpassed that of DE-NPs, while DE-NPs were able to load more kinds of proteins. In addition, the stability of NP was possible to further modulate simply by incorporating other types of hydrazide residues in the biodynamer. Despite the pronounced influence of formulation methodologies on D_H, morphology, drug loading, stability, and cellular uptake efficiency, both PNCs and DE-NPs maintained their intrinsic pH-responsive degradation natures and exhibited exemplary biocompatibility. Even when biodynamer facilitates two entirely distinct formulation methods, the unique demands of each application warrant careful consideration in the choice of formulation approach.

The development of precision-engineered PNCs and DE-NPs for delivering functional proteins holds immense potential not only in therapeutic applications but also within the biotechnological landscape. Notably, charged PNCs have exhibited noteworthy encapsulation efficiency, while DE-NPs have manifested a spherical morphology, thereby augmenting their intracellular delivery capabilities. Despite these promising attributes, certain challenges persist, necessitating further investigation. Unforeseen functional variations, such as immunogenic host reactions and long-term stability concerns, underscore the need for continued research. Rigorous efforts are imperative to comprehensively assess safety profiles and delivery efficiencies in vivo.

In conclusion, our biodynamers offer a sophisticated, pH-responsive delivery platform for protein drugs. This innovation holds significant promise for controlled release and targeted delivery of functional protein cargoes,

particularly antibodies. As we move forward, continued research and refinement are essential to unlock the full potential of these advanced delivery systems.

Acknowledgments

Author Contributions

All authors made a significant contribution to the work reported, whether that is in the conception, study design, execution, acquisition of data, analysis and interpretation, or in all these areas; took part in drafting, revising or critically reviewing the article; gave final approval of the version to be published; have agreed on the journal to which the article has been submitted; and agree to be accountable for all aspects of the work.

Disclosure

WO2021259783A1 (EP3928798A1) was filed in relation to the article. The authors report no other conflicts of interest in this work.

References

1. Lv J, Fan Q, Wang H, Cheng Y. Polymers for cytosolic protein delivery. *Biomaterials*. 2019;218:119358. doi:10.1016/j.biomaterials.2019.119358
2. Viegas C, Seck F, Fonte P. An insight on lipid nanoparticles for therapeutic proteins delivery. *J Drug Delivery Sci Technol*. 2022;77:103839. doi:10.1016/j.jddst.2022.103839
3. Olshefsky A, Richardson C, Pun SH, King NP. Engineering self-assembling protein nanoparticles for therapeutic delivery. *Bioconjugate Chem*. 2022;33(11):2018–2034. doi:10.1021/acs.bioconjchem.2c00030
4. Li Y, Ye Z, Yang H, Xu Q. Tailoring combinatorial lipid nanoparticles for intracellular delivery of nucleic acids, proteins, and drugs. *Acta Pharm Sin B*. 2022;12(6):2624–2639. doi:10.1016/j.apsb.2022.04.013
5. Ashok B, Peppas NA, Wechsler ME. Lipid- and polymer-based nanoparticle systems for the delivery of CRISPR/Cas9. *J Drug Delivery Sci Technol*. 2021;65. doi:10.1016/j.jddst.2021.102728
6. Le Saux S, Aubert-Pouëssel A, Ouchait L, et al. Nanotechnologies for intracellular protein delivery: recent progress in inorganic and organic nanocarriers. *Adv Ther*. 2021;4(6):2100009. doi:10.1002/adtp.202100009
7. Zhang T, Xu J, Chen J, Wang Z, Wang X, Zhong J. Protein nanoparticles for Pickering emulsions: a comprehensive review on their shapes, preparation methods, and modification methods. *Trends Food Sci Technol*. 2021;113:26–41. doi:10.1016/j.tifs.2021.04.054
8. Zhou H-X, Pang X. Electrostatic interactions in protein structure, folding, binding, and condensation. *Chem Rev*. 2018;118(4):1691–1741. doi:10.1021/acs.chemrev.7b00305
9. Yang X, Wang Y, Zhao J, et al. Coordinated regulation of BACH1 and mitochondrial metabolism through tumor-targeted self-assembled nanoparticles for effective triple negative breast cancer combination therapy. *Acta Pharm Sin B*. 2022;12(10):3934–3951. doi:10.1016/j.apsb.2022.06.009
10. Van der Vegt NFA, Nayar D. The hydrophobic effect and the role of cosolvents. *Phys Chem B*. 2017;121(43):9986–9998. doi:10.1021/acs.jpcb.7b06453
11. Zhuang W-R, Wang Y, Cui P-F, et al. Applications of π-π stacking interactions in the design of drug-delivery systems. *J Controlled Release*. 2019;294:311–326. doi:10.1016/j.jconrel.2018.12.014
12. McClements DJ, Jafari SM. Improving emulsion formation, stability and performance using mixed emulsifiers: a review. *Adv Colloid Interface Sci*. 2018;251:55–79. doi:10.1016/j.cis.2017.12.001
13. Crucho CIC, Barros MT. Polymeric nanoparticles: a study on the preparation variables and characterization methods. *Mater Sci Eng C*. 2017;80:771–784. doi:10.1016/j.msec.2017.06.004
14. Sharma S, Parmar A, Kori S, Sandhir R. PLGA-based nanoparticles: a new paradigm in biomedical applications. *Trac Trends Anal Chem*. 2016;80 (2):30–40. doi:10.1016/j.trac.2015.06.014
15. Saffarionpour S. One-step preparation of double emulsions stabilized with amphiphilic and stimuli-responsive block copolymers and nanoparticles for nutraceuticals and drug delivery. *JCIS Open*. 2021;3(2):100020. doi:10.1016/j.jciso.2021.100020
16. McClements DJ, Decker EA, Weiss J. Emulsion-based delivery systems for lipophilic bioactive components. *J Food Sci*. 2007;72(8):R109–24. doi:10.1111/j.1750-3841.2007.00507.x
17. Hanson JA, Chang CB, Graves SM, Li Z, Mason TG, Deming TJ. Nanoscale double emulsions stabilized by single-component block copolypeptides. *Nature*. 2008;455(7209):85–88. doi:10.1038/nature07197
18. Zhao S, Huang C, Yue X, et al. Application advance of electrosprayed micro/nanoparticles based on natural or synthetic polymers for drug delivery system. *Mater Des*. 2022;220(2):110850. doi:10.1016/j.matdes.2022.110850
19. Liu Y, Stuart MCA, Buhler E, Lehn J-M, Hirsch AKH. Proteoid dynamers with tunable properties. *Adv Funct Mater*. 2016;26(34):6297–6305. doi:10.1002/adfm.201601612

20. Liu Y, Lehn J-M, Hirsch AKH. Molecular biodynamers: dynamic covalent analogues of biopolymers. *Acc Chem Res*. 2017;50(2):376–386. doi:10.1021/acs.accounts.6b00594

21. Ding H, Tan P, Fu S, et al. Preparation and application of pH-responsive drug delivery systems. *J Controlled Release*. 2022;348:206–238. doi:10.1016/j.jconrel.2022.05.056

22. Hu Y, Ruan X, Lv X, et al. Biofilm microenvironment-responsive nanoparticles for the treatment of bacterial infection. *Nano Today*. 2022;46 (1):101602. doi:10.1016/j.nantod.2022.101602

23. Socea L-I, Barbuceanu S-F, Pahontu EM, et al. Acylhydrazones and Their Biological Activity: a Review. *Molecules*. 2022;27(24). doi:10.3390/molecules27248719

24. Hirsch AKH, Buhler E, Lehn J-M. Biodynamers: self-organization-driven formation of doubly dynamic proteoids. *J Am Chem Soc*. 2012;134 (9):4177–4183. doi:10.1021/ja2099134

25. Xiong X-B, Binkhathlan Z, Molavi O, Lavasanifar A. Amphiphilic block co-polymers: preparation and application in nanodrug and gene delivery. *Acta Biomater*. 2012;8(6):2017–2033. doi:10.1016/j.actbio.2012.03.006

26. Panta P, Kim DY, Kwon JS, Son AR, Lee KW, Kim MS. Protein drug-loaded polymeric nanoparticles. *JBiSE*. 2014;07(10):825–832. doi:10.4236/jbise.2014.710082

27. Zhao H, Lin ZY, Yildirimer L, Dhinakar A, Zhao X, Wu J. Polymer-based nanoparticles for protein delivery: design, strategies and applications. *J Mater Chem B*. 2016;4(23):4060–4071. doi:10.1039/C6TB00308G

28. Wu J, Sahoo JK, Li Y, Xu Q, Kaplan DL. Challenges in delivering therapeutic peptides and proteins: a silk-based solution. *J Controlled Release*. 2022;345:176–189. doi:10.1016/j.jconrel.2022.02.011

29. Elmowafy M, Shalaby K, Elkomy MH, et al. Polymeric nanoparticles for delivery of natural bioactive agents: recent advances and challenges. *Polymers*. 2023;15(5). doi:10.3390/polym15051123

30. Wang X, Shi C, Wang L, Luo J. Polycation-telodendrimer nanocomplexes for intracellular protein delivery. *Colloids Surf B Biointerfaces*. 2018;162:405–414. doi:10.1016/j.colsurfb.2017.12.021

31. Yukuyama MN, Kato ETM, Lobenberg R, Bou-Chacra NA. Challenges and future prospects of nanoemulsion as a drug delivery system. *Curr Pharm Des*. 2017;23(3):495–508. doi:10.2174/1381612822666161027111957

32. Bizeau J, Mertz D. Design and applications of protein delivery systems in nanomedicine and tissue engineering. *Adv Colloid Interface Sci*. 2021;287:102334. doi:10.1016/j.cis.2020.102334

33. Kleynhans J, Sathekge M, Ebenhan T. Obstacles and recommendations for clinical translation of nanoparticle system-based targeted alpha-particle therapy. *Materials*. 2021;14(17). doi:10.3390/ma14174784

34. Zhang Y, Guo Y, Liu F, Luo Y. Recent development of egg protein fractions and individual proteins as encapsulant materials for delivery of bioactives. *Food Chem*. 2023;403:134353. doi:10.1016/j.foodchem.2022.134353

35. Gao X, He C, Xiao C, Zhuang X, Chen X. Biodegradable pH-responsive polyacrylic acid derivative hydrogels with tunable swelling behavior for oral delivery of insulin. *Polymer*. 2013;54(7):1786–1793. doi:10.1016/j.polymer.2013.01.050

36. Lu Y, Sun W, Gu Z. Stimuli-responsive nanomaterials for therapeutic protein delivery. *J Control Release*. 2014;194:1–19. doi:10.1016/j.jconrel.2014.08.015

37. Yang T, Sun D, Xu P, et al. Stability of bovine serum albumin labelled by rhodamine B isothiocyanate. *Biomed Res*. 2017;28(9):3851–3854.

38. Czuba E, Diop M, Mura C, et al. Oral insulin delivery, the challenge to increase insulin bioavailability: influence of surface charge in nanoparticle system. *Int J Pharm*. 2018;542(1–2):47–55. doi:10.1016/j.ijpharm.2018.02.045

39. Wilson BK, Prud'homme RK. Nanoparticle size distribution quantification from transmission electron microscopy (TEM) of ruthenium tetroxide stained polymeric nanoparticles. *J Colloid Interface Sci*. 2021;604:208–220. doi:10.1016/j.jcis.2021.04.081

40. Discher DE, Ahmed F. Polymersomes. *Annu Rev Biomed Eng*. 2006;8:323–341. doi:10.1146/annurev.bioeng.8.061505.095838

41. Caputo F, Clogston J, Calzolai L, Rösslein M, Prina-Mello A. Measuring particle size distribution of nanoparticle enabled medicinal products, the joint view of EUNCL and NCI-NCL. A step by step approach combining orthogonal measurements with increasing complexity. *J Controlled Release*. 2019;299:31–43. doi:10.1016/j.jconrel.2019.02.030

42. Shen S, Wu Y, Liu Y, Wu D. High drug-loading nanomedicines: progress, current status, and prospects. *Int J Nanomedicine*. 2017;12:4085–4109. doi:10.2147/IJN.S132780

43. Haim Zada M, Rottenberg Y, Domb AJ. Peptide loaded polymeric nanoparticles by non-aqueous nanoprecipitation. *J Colloid Interface Sci*. 2022;622:904–913. doi:10.1016/j.jcis.2022.05.007

44. Hickey JW, Santos JL, Williford J-M, Mao H-Q. Control of polymeric nanoparticle size to improve therapeutic delivery. *J Control Release*. 2015;219:536–547. doi:10.1016/j.jconrel.2015.10.006

45. Yang -Q-Q, Cai W-Q, Wang Z-X, et al. Structural characteristics, binding behaviors, and stability of ternary nanocomplexes of lecithin, polyvinylpyrrolidone, and curcumin. *LWT*. 2023;175(12):114489. doi:10.1016/j.lwt.2023.114489

46. Insua I, Wilkinson A, Fernandez-Trillo F. Polyion complex (PIC) particles: preparation and biomedical applications. *Eur Polym J*. 2016;81:198–215. doi:10.1016/j.eurpolymj.2016.06.003

47. Rehmani S, McLaughlin CM, Eltaher HM, Moffett RC, Flatt PR, Dixon JE. Orally-delivered insulin-peptide nanocomplexes enhance transcytosis from cellular depots and improve diabetic blood glucose control. *J. Controlled Release*. 2023;360:93–109. doi:10.1016/j.jconrel.2023.06.006

48. Niu Z, Samaridou E, Jaumain E, et al. PEG-PGA enveloped octaarginine-peptide nanocomplexes: an oral peptide delivery strategy. *J. Controlled Release*. 2018;276:125–139. doi:10.1016/j.jconrel.2018.03.004

49. Pochapski DJ, Carvalho Dos Santos C, Leite GW, Pulcinelli SH, Santilli CV. Zeta potential and colloidal stability predictions for inorganic nanoparticle dispersions: effects of experimental conditions and electrokinetic models on the interpretation of results. *Langmuir*. 2021;37 (45):13379–13389. doi:10.1021/acs.langmuir.1c02056

50. Sun T, Jiang C. Stimuli-responsive drug delivery systems triggered by intracellular or subcellular microenvironments. *Adv Drug Deliv Rev*. 2023;196:114773. doi:10.1016/j.addr.2023.114773

51. Wu W, Luo L, Wang Y, et al. Endogenous pH-responsive nanoparticles with programmable size changes for targeted tumor therapy and imaging applications. *Theranostics*. 2018;8(11):3038–3058. doi:10.7150/thno.23459

52. Panigrahi D, Sahu PK, Swain S, Verma RK. Quality by design prospects of pharmaceuticals application of double emulsion method for PLGA loaded nanoparticles. *SN Appl Sci*. 2021;3(6):15. doi:10.1007/s42452-021-04609-1

53. Liu Y, Tan J, Thomas A, Ou-Yang D, Muzykantov VR. The shape of things to come: importance of design in nanotechnology for drug delivery. *Ther Deliv*. 2012;3(2):181–194. doi:10.4155/tde.11.156

54. Cooley M, Sarode A, Hoore M, Fedosov DA, Mitragotri S, Sen Gupta A. Influence of particle size and shape on their margination and wall-adhesion: implications in drug delivery vehicle design across nano-to-micro scale. *Nanoscale*. 2018;10(32):15350–15364. doi:10.1039/C8NR04042G

55. Champion JA, Mitragotri S. Role of target geometry in phagocytosis. *Proc Natl Acad Sci U S A*. 2006;103(13):4930–4934. doi:10.1073/pnas.0600997103

56. Zhang K, Fang H, Chen Z, Taylor J-SA, Wooley KL. Shape effects of nanoparticles conjugated with cell-penetrating peptides (HIV Tat PTD) on CHO cell uptake. *Bioconjug Chem*. 2008;19(9):1880–1887. doi:10.1021/bc800160b

57. Kapate N, Clegg JR, Mitragotri S. Non-spherical micro- and nanoparticles for drug delivery: progress over 15 years. *Adv Drug Deliv Rev*. 2021;177:113807. doi:10.1016/j.addr.2021.05.017

58. Safari H, Felder ML, Kaczorowski N, Eniola-Adefeso O. Effect of the emulsion solvent evaporation technique cosolvent choice on the loading efficiency and release profile of anti-CD47 from PLGA Nanospheres. *J Pharm Sci*. 2022;111(9):2525–2530. doi:10.1016/j.xphs.2022.04.007

59. Lagreca E, Onesto V, Di Natale C, La Manna S, Netti PA, Vecchione R. Recent advances in the formulation of PLGA microparticles for controlled drug delivery. *Prog Biomater*. 2020;9(4):153–174. doi:10.1007/s40204-020-00139-y

60. Mitchell MJ, Billingsley MM, Haley RM, Wechsler ME, Peppas NA, Langer R. Engineering precision nanoparticles for drug delivery. *Nat Rev Drug Discov*. 2021;20(2):101–124. doi:10.1038/s41573-020-0090-8

61. Ghitman J, Biru EI, Stan R, Iovu H. Review of hybrid PLGA nanoparticles: future of smart drug delivery and theranostics medicine. *Materials Design*. 2020;193(1):108805. doi:10.1016/j.matdes.2020.108805

62. Han L, Lu K, Zhou S, Qi B, Li Y. Co-delivery of insulin and quercetin in W/O/W double emulsions stabilized by different hydrophilic emulsifiers. *Food Chem*. 2022;369:130918. doi:10.1016/j.foodchem.2021.130918

63. Jarudilokkul S, Tongthammachat A, Boonamnuayvittaya V. Preparation of chitosan nanoparticles for encapsulation and release of protein. *Korean J Chem Eng*. 2011;28(5):1247–1251. doi:10.1007/s11814-010-0485-z

64. Di Martino A, Kucharczyk P, Capakova Z, Humpolicek P, Sedlarik V. Chitosan-based nanocomplexes for simultaneous loading, burst reduction and controlled release of doxorubicin and 5-fluorouracil. *Int J Biol Macromol*. 2017;102:613–624. doi:10.1016/j.ijbiomac.2017.04.004

65. McCall RL, Sirianni RW. PLGA nanoparticles formed by single- or double-emulsion with vitamin E-TPGS. *J Vis Exp*. 2013;82:51015. doi:10.3791/51015

66. Leibrock L, Wagener S, Singh AV, Laux P, Luch A. Nanoparticle induced barrier function assessment at liquid-liquid and air-liquid interface in novel human lung epithelia cell lines. *Toxicol Res*. 2019;8(6):1016–1027. doi:10.1039/C9TX00179D

67. Barosova H, Meldrum K, Karakocak BB, et al. Inter-laboratory variability of A549 epithelial cells grown under submerged and air-liquid interface conditions. *Toxicol In Vitro*. 2021;75:105178. doi:10.1016/j.tiv.2021.105178

68. Issa Y, Watts DC, Brunton PA, Waters CM, Duxbury AJ. Resin composite monomers alter MTT and LDH activity of human gingival fibroblasts in vitro. *Dent Mater*. 2004;20(1):12–20. doi:10.1016/S0109-5641(03)00053-8

69. Zheng J, Fang X, Li L, Zhang R, Li C. Biomolecule-responsive nanoprobes for living cell analysis. *TrAC Trends in Analytical Chemistry*. 2023;169(4):117387. doi:10.1016/j.trac.2023.117387

70. Chen B, Liu L, Yue R, et al. Stimuli-responsive switchable MRI nanoprobe for tumor theranostics. *Nano Today*. 2023;51:101931. doi:10.1016/j.nantod.2023.101931

71. Banach Ł, Williams GT, Fossey JS. Insulin delivery using dynamic covalent boronic acid/ester-controlled release. *Adv Therap*. 2021;4(11):S11. doi:10.1002/adtp.202100118

72. Sun P, Jiao J, Wang X, et al. Nanomedicine hybrid and catechol functionalized chitosan as pH-responsive multi-function hydrogel to efficiently promote infection wound healing. *Int J Biol Macromol*. 2023;238:124106. doi:10.1016/j.ijbiomac.2023.124106

73. Li D, Tang G, Yao H, et al. Formulation of pH-responsive PEGylated nanoparticles with high drug loading capacity and programmable drug release for enhanced antibacterial activity. *Bioact Mater*. 2022;16:47–56. doi:10.1016/j.bioactmat.2022.02.018

74. Tang Z, He C, Tian H, et al. Polymeric nanostructured materials for biomedical applications. *Progress in Polymer Science*. 2016;60(Suppl. 24):86–128. doi:10.1016/j.progpolymsci.2016.05.005